

Diffusion reordering kinetics in lattice-gas systems: Time evolution of configurational entropy and internal energy

Sieghard Weinketz

Institut für Computeranwendungen 1, Universität Stuttgart, Pfaffenwaldring 27, D-70569 Stuttgart, Germany

(Received 3 February 1998)

The reordering kinetics of a diffusion lattice-gas system of adsorbates with nearest- and next-nearest-neighbor interactions on a square lattice is studied within a dynamic Monte Carlo simulation, as it evolves towards the equilibrium from a given initial configuration, at a constant temperature. The diffusion kinetics proceeds through adsorbate hoppings to empty nearest-neighboring sites (Kawasaki dynamics). The Monte Carlo procedure allows a “real” time definition from the local transition rates, and the configurational entropy and internal energy can be obtained from the lattice configuration at any instant t by counting the local clusters and using the C_2 approximation of the cluster variation method. These state functions are then used in their nonequilibrium form as a direct measure of reordering along the time. Different reordering processes are analyzed within this approach, presenting a rich variety of behaviors. It can also be shown that the time derivative of entropy (times temperature) is always *equal to or lower than* the time derivative of energy, and that the reordering path is always strongly dependent on the initial order, presenting in some cases an “invariance” of the entropy function to the magnitude of the interactions as far as the final order is unaltered. [S1063-651X(98)02507-0]

PACS number(s): 05.70.Ln, 68.35.Fx, 82.20.Mj, 64.60.Ht

I. INTRODUCTION

Kinetic lattice-gas models with stochastic interactions have been widely used in the study of the diffusion of adsorbates over metallic surfaces [1–11], where a low activation energy makes the diffusion process very fast with respect to processes like desorption or adsorption [12]. These studies were mostly concerned with diffusion as a mass transport due to a concentration gradient [2–4], in obtaining diffusion coefficients within an equilibrium condition [5–9], or in the case of diffusion kinetics driven by an external field [10,11]. A rather different issue, however, is the reordering kinetics of an adsorbed layer or lattice gas as it converges to the equilibrium from an arbitrary initial order, and this leads to the question of how the reordering process can be expressed into the order parameters and the (nonequilibrium) thermodynamic state functions. A similar problem was studied by Smith and Zangwill [13] for the reordering kinetics of a binary lattice gas in two dimensions, using a time-dependent quasichemical approximation.

A good knowledge of the reordering kinetics of adsorbates will be important when understanding its relation to the time scales of other processes like desorption or adsorption of atoms and molecules, that is normally treated within the assumption that diffusion is sufficiently rapid so that the adsorbate layer can be considered to be instantaneously in equilibrium [14–16]. The equilibrium state of lattice gases can be properly described by different numerical-analytical [17–19] or Monte Carlo methods [16,20–22].

The equilibrium state of a thermodynamic system is by definition the minimum of the Helmholtz free energy F [23]:

$$F = E - TS,$$

where E is the internal energy and S is the configurational

entropy. By assuming that F converges to its minimum *monotonically* from its initial value, we may find for its time derivative,

$$\frac{\partial F}{\partial t} = \frac{\partial E}{\partial t} - T \frac{\partial S}{\partial t} \leq 0,$$

which leads to the constraint

$$\frac{\partial E}{\partial t} \leq T \frac{\partial S}{\partial t}. \quad (1)$$

In this way that we can speak of an *entropy dominated* regime, whenever $T|\partial S/\partial t| < |\partial E/\partial t|$, or otherwise of an *energy dominated* regime, and the latter will occur when *both* state functions are decreasing with time. There is one situation that may occur whenever the system is near equilibrium, with $\partial F/\partial t \approx 0$, that is,

$$\frac{\partial E}{\partial t} \approx T \frac{\partial S}{\partial t}. \quad (2)$$

In this work we will study, as a simple system that can exhibit reordering kinetics, the lattice-gas model of adsorbates over a square lattice with nearest- and next-nearest-neighbor interactions between the adsorbates, and where the diffusion of the adsorbates occurs by thermally activated “jumps” from filled to empty surface sites at a constant temperature (thermal bath), following a Kawasaki dynamics. The jump rates depend directly on the activation energies for hopping as a function of the differences between the initial and final energies for the jumps.

The time evolution of the system can be evaluated within a dynamic Monte Carlo procedure [25,26], considering the stochastic process as a heterogeneous Poisson process composed by all the local *possible events* present in the system at

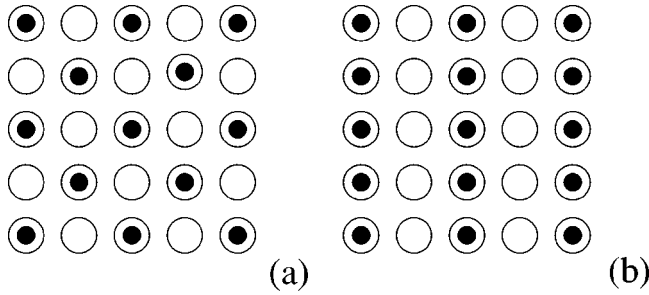


FIG. 1. The ordered states $c(2 \times 2)$ (a) and $p(2 \times 1)$ (b), corresponding to zero entropy values.

a given instant. Moreover, from a direct counting of the local cluster correlations, the entropy and the energy can be directly evaluated at any instant t with the use of the formulas from the C_2 approximation of the cluster variation method [18], as the ordering process proceeds from the initial ordered states towards the equilibrium states. Two important cases to be addressed here are the ones with energy parameters that correspond to the $c(2 \times 2)$ (or “checkerboard”) [16,19–21] and $p(2 \times 1)$ [9,11] equilibrium states (Fig. 1), which are both ordered states with corresponding zero entropy. In this way we can show that the ordering kinetics will depend not only on the final state but also on the initial order, being eventually independent from the energy parameters as long as the equilibrium state is unchanged. Finally, the constraint derived above [Eq. (1)] for the relation between the time derivatives of entropy and internal energy can be verified in the simulations.

The diffusion model and the dynamic Monte Carlo procedure are described in Sec. II, and the internal energy and configurational entropy formulas based on the C_2 approximation of the cluster variation method, as well as the cluster fractions used in their derivation are presented in Sec. III. In Sec. IV we will present some examples of reordering processes, showing the interplay between the two thermodynamic functions, with different energy parameters and initial configurations. The discussion will be limited to the half-coverage case, and to repulsive energies, for that is where most interesting phase transitions can be observed [20,21]. Final discussions and conclusions are presented in Sec. V.

II. DIFFUSION MODEL AND MONTE CARLO PROCEDURE

The solid surface is represented by a square lattice with N_s sites and periodic boundary conditions, where each site may be either empty or occupied by an adsorbate. The total number of adsorbates on the surface is given by N_A , defining a surface coverage $\theta = N_A/N_s$. Only diffusion events (hopping) of an adsorbate to empty nearest-neighbor sites (Kawasaki dynamics) are included in the model; all other processes such as desorption or adsorption processes are ignored.

The equilibrium state that is to be reached by the diffusion process can be characterized by two parameter ratios, $\Delta_l/k_B T$ and $\Delta_d/k_B T$, where Δ_l and Δ_d are, respectively, the nearest-neighbor (lateral) and next-nearest-neighbor (diagonal) interaction energies between the adsorbates (repulsive energies positively defined), k_B is the Boltzmann constant,

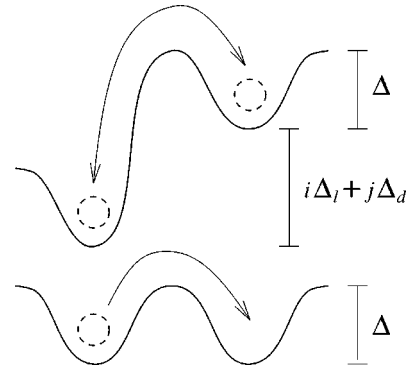


FIG. 2. Barrier heights (activation energies) for adsorbate jumps between sites of different initial and final energies. Δ is the barrier height in the limit of zero coverage, and $i\Delta_l + j\Delta_d$ is the difference in total energy for the adsorbate between the initial and final sites. Note that the barrier height for equal or lower energy final sites is just Δ [Eq. (3)].

and T is the absolute temperature. By assuming an Arrhenius form for the hopping rate, two further parameters are needed, the pre-exponential factor for diffusion, ν , and the activation energy in the absence of neighbor interactions, Δ , and therefore the hopping rates for an adsorbate between two neighboring sites with final energy differences labeled by ij are given by

$$r_{\text{diff}}^{ij} = \nu \exp[-(\Delta + i\Delta_l + j\Delta_d)/k_B T] \quad (3a)$$

if $i\Delta_l + j\Delta_d > 0$, and

$$r_{\text{diff}}^{ij} = \nu \exp(-\Delta/k_B T) \quad (3b)$$

if $i\Delta_l + j\Delta_d \leq 0$, where i and j are, respectively, the *differences* in the numbers of nearest and next-nearest neighbors for the adsorbate between its initial and final sites ($-3 \leq i \leq 3, -4 \leq j \leq 4$), following the physicochemical argument that the energy barrier the adsorbate effectively “feels” when jumping onto a lower energy site is just Δ (Fig. 2) [27]. By ignoring the kinetics involved, the transition rates (3a) and (3b) become equivalent to the rules of the Metropolis algorithm [24], what by analogy guarantees that the system will converge after sufficient computing time to an equilibrium state.

The time evolution of the system can be obtained within the dynamic Monte Carlo procedure [25,26] from the local transition rates by considering a heterogeneous Poisson process [25,28]. Therefore, for a given configuration at an instant t , a *global transition rate* for the next diffusion event is given by

$$r_{\text{tot}} = \sum_{ij} N_{\text{diff}}^{ij} r_{\text{diff}}^{ij}, \quad (4)$$

where N_{diff}^{ij} are the numbers (multiplicities) of the *possible diffusion events* with environment dependence labeled by ij . The next event to occur is then randomly chosen out of a weighted list of all the $N_{\text{tot}} = \sum_{ij} N_{\text{diff}}^{ij}$ existing possibilities [30]. This diffusion event is then performed, and the surface lattice, the list of possible events, and the multiplicities N_{diff}^{ij} are updated, and the time t is incremented according to

$$\tau_{\text{inc}} = (-\ln \rho) \frac{1}{r_{\text{tot}}}, \quad (5)$$

where ρ is a nonzero random number between 0 and 1 [31]. The sequence of lattice configurations generated in this way is a *representative solution* of the time evolution of the kinetic lattice-gas model, and any system variable can be directly measured from the lattice configuration.

From the transition rates in Eq. (3), and from Eqs. (4) and (5), it is possible to see that the time increment will be always inversely proportional to $\nu \exp(-\Delta/k_B T)$, and that this term will be constant throughout the whole process as long as T is kept constant. Therefore, for practical reasons and in order to evaluate the influence of adsorbate interactions in the reordering kinetics, the time evolution will be measured in units of $1/[\nu \exp(-\Delta/k_B T)]$.

III. CONFIGURATIONAL ENTROPY AND INTERNAL ENERGY IN THE C_2 APPROXIMATION

The configurational entropy and the internal energy can be directly obtained from the lattice configuration at a given instant t . The internal energy is the simplest case, and it can be directly obtained from the probabilities y_1 that two nearest neighboring sites are occupied, and w_1 , that two next-nearest-neighboring sites are occupied (Table I), so that for a lattice with N_s sites the internal energy (per unit site) is

$$E = 2(y_1 \Delta_l + w_1 \Delta_d), \quad (6)$$


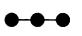

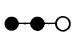
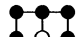
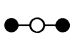

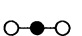

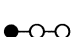

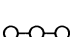
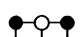
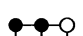

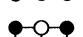


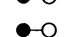

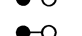

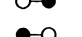

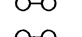
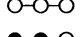
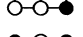

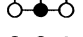

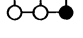

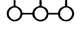
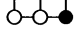

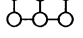

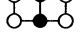
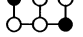

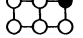
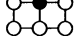
where the binding energy term was ignored as it is irrelevant for the kinetics.

The configurational entropy, on the other hand, relies on using an appropriate approximation that can describe the local order correlations of a lattice-gas system at a given coverage, temperature, and interaction terms *in the equilibrium state*. This can be achieved by the cluster variation method (CVM) [17,18], which gives a series of cluster approximations for the configurational entropy of an infinite lattice as a function of the basic cluster fractions, with the precision of the approximation depending on the size of the basic cluster, their geometry and the way they are used to construct an infinite lattice. The equilibrium state can then be found as the minimum of the free energy by varying self-consistently the cluster probabilities [32]. In a previous work we found that the C_2 approximation of Kikuchi and Brush [18] was sufficiently precise to describe the $c(2 \times 2)$ ordering transition at half coverage by comparing to Monte Carlo simulations [16]. By following the procedure outlined for the B_2 approximation in Ref. [18], we arrive at the configurational entropy (per unit site) as

$$S = k_B \left\{ \sum_i \kappa_i q_i \ln q_i + \sum_i \tau_i t_i \ln t_i - \sum_i \beta_i y_i \ln y_i - \sum_i \eta_i h_i \ln h_i \right\}, \quad (7)$$

where the q_i , t_i , y_i , and h_i cluster probabilities are presented in Table I, with their respective multiplicities or sym-

TABLE I. Basic (h_i) and secondary cluster (q_i , t_i , and y_i), with their respective multiplicities (η_i , κ_i , τ_i , and β_i) used in the C_2 approximation of the cluster variation method. The w_1 fraction does not enter the entropy formula, but is used in the energy calculation.

	h_1	1		q_1	1
	h_2	4		q_2	2
	h_3	2		q_3	1
	h_4	2		q_4	1
	h_5	4		q_5	2
	h_6	2		q_1	1
	h_7	4			
	h_8	2		t_1	1
	h_9	1		t_2	4
	h_{10}	4		t_3	4
	h_{11}	4		t_4	2
	h_{12}	4		t_5	4
	h_{13}	2		t_6	1
	h_{14}	4			
	h_{15}	2		y_1	1
	h_{16}	2		y_2	2
	h_{17}	4		y_3	1
	h_{18}	4			
	h_{19}	2		x_1	1
	h_{20}	1		x_2	1
	h_{21}	2			
	h_{22}	4		w_1	
	h_{23}	2			
	h_{24}	1			

metry factors κ_i , τ_i , β_i , and η_i . This formula will then be used here for the *nonequilibrium* entropy.

The y_i , q_i , and t_i fractions can be obtained in different ways as geometrical sums over the h_i clusters by considering their geometries, and the same is valid for w_1 in Eq. (6). The cluster probabilities satisfy the normalization constraints

$$\sum_i \eta_i h_i = \sum_i \kappa_i q_i = \sum_i \tau_i t_i = \sum_i \beta_i y_i = 1,$$

and also

$$y_1 + y_2 = x_1 = \theta.$$

For the cluster fractions at a given instant t , the lattice is scanned in the two perpendicular directions and each of the $2N_s$ (3×2) clusters is then recognized and counted as one of the h_i figures of Table I (accounting also for their symmetries), and the h_i fractions are then obtained by dividing the corresponding figure counts by $2N_s \eta_i$. The q_i , t_i , y_i , and w_i fractions are obtained as geometrical sums over the h_i fractions, and finally E and S are obtained with the use of formulas (6) and (7). The direct use of Eq. (7) can lead to errors in the entropy evaluation, as it was in fact devised for infinite lattices, and especially in the neighborhood of the highly asymmetrical $p(2 \times 2)$ orders. A numerical solution employed here was to calculate the entropy separately from the cluster counts for each direction of the lattice, and this avoids the negative values in the entropy.

An important issue to be concerned with here is that of the validity and significance of the configurational entropy (7). The entropy is a well defined function in the equilibrium state, and its derivation in Ref. [18] was done by estimating the number of different ways that an N_s -site lattice can be built with the use of the given cluster probabilities. This means that an entropy S will correspond to a given lattice configuration as long as this cluster is representative of an ensemble of lattices built with these cluster probabilities (Gibbs-like description).

This should not be very severe in our case, as we are dealing mostly with local reordering processes that do not involve mass transport. Furthermore, the entropy can always be seen as a function that measures the degree disorder of the system as a function of its local probabilities or correlations, as in the approach given by the information theory [33] (Boltzmann-like description). In this way, the entropy is a consistent function of the cluster probabilities that will converge to its equilibrium value as the stochastic system converges to the equilibrium.

IV. SIMULATION OF REORDERING PROCESSES

The simplest case that can be studied within the procedure outlined above is the disordering process from an initially ordered state to a final random state, due to the absence of interactions between the adsorbates ($\Delta_l = \Delta_d = 0$). In Fig. 3 we show the convergence of the entropy towards its maximum value of $S = k_B \ln 2$, starting from the two ordered states shown in Fig. 1: $c(2 \times 2)$ (solid line) and $p(2 \times 1)$ (dashed line), for a system at half coverage. For this and all the following figures in this work we use, unless otherwise stated, $N_s = 400 \times 400$, $\theta = 0.5$, and $T = 300$ K, with the Boltzmann constant $k_B = 0.8617 \times 10^{-4}$ eV/K. The time is measured in units of $1/[\nu \exp(-\Delta/k_B T)]$, as previously mentioned. The code was written in PASCAL language and was run on Sun ULTRA 1 workstations.

It can be seen that both curves show saturationlike behavior for S , but noting that the convergence from the initial

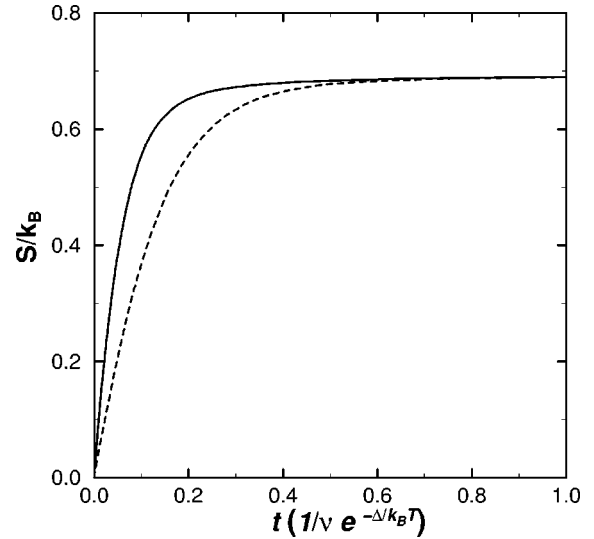


FIG. 3. Time evolution of the configuration entropy in the absence of adsorbate-adsorbate interactions ($\Delta_l = \Delta_d = 0$), in units of $\nu \exp(-\Delta_l/k_B T)$, for initial states in the $c(2 \times 2)$ (solid) and $p(2 \times 1)$ orders (dashed line). Both curves converge to the plateau $S/k_B = \ln 2$.

$c(2 \times 2)$ order is quite faster. This comes from the restriction that the adsorbates may only jump to empty nearest-neighboring sites, which means that an adsorbate in an ordered $p(2 \times 1)$ row has just two hopping possibilities, whereas an adsorbate in the $c(2 \times 2)$ order has four possibilities (Fig. 1), which allows a faster destruction of the original order in the initial stages. This situation is the only example within this model of a thermodynamically closed system, due to its constant internal energy, implying that all the change upon the free energy comes from the entropy.

A rather different situation occurs for $\Delta_l = 2\Delta_d = 0.1$ eV, where each of the interaction terms would individually lead to either the $c(2 \times 2)$ or $p(2 \times 1)$ orders. This is shown in Fig. 4 for both the internal energies (upper set of curves) and entropies (lower set), where at $t=0$ the system is posed into a $c(2 \times 2)$ (thick solid), $p(2 \times 1)$ (thin solid), or random disorder state (dashed line), and all the curves in each set converge to same values. It can be seen that the overall time scale is rather larger than that of Fig. 3. Again, the convergence from the initial $c(2 \times 2)$ is faster than that of $p(2 \times 1)$ during the initial stages, for the same reason as with the previous case, but a direct comparison for the curve with initial random order cannot be made.

The time derivatives of the curves in Fig. 4 were obtained with the use of a Savitzky-Golay smoothing procedure [29] and are presented in Fig. 5 for each of the initial orders (the solid lines correspond here to the internal energy, and the dashed lines to the entropy). It can be seen that condition (1) is fulfilled, which can be interpreted as if the change in internal energy “pulls” the change in entropy. For the larger values of t , when the system is close to equilibrium, the two curves practically superpose and follow the same oscillations, satisfying thus condition (2). The oscillations arise from the stochastic processes involved here, and are amplified by the limited size of the lattice. Note also the differences in vertical scales for the three cases.

An important case to be considered here and frequently

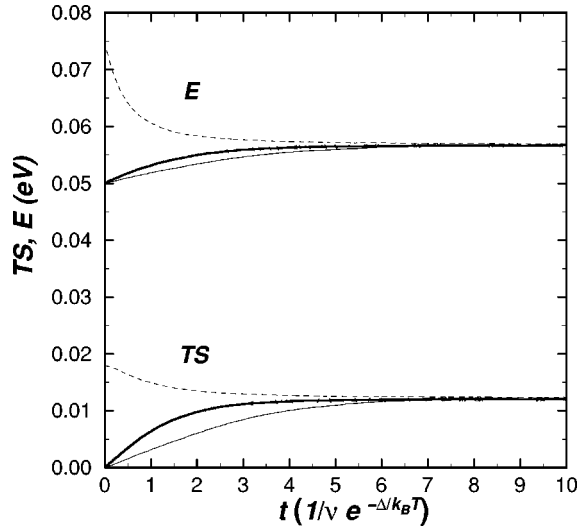


FIG. 4. Time evolution of the entropy (lower set) and internal energy functions (upper set) for $\Delta_l=0.1$ eV and $\Delta_d=0.05$ eV, for the lattices at initial states of $c(2\times 2)$ (thick solid), $p(2\times 1)$ (thin solid), and randomly disordered (dashed line). $T=300$ K, as in all the subsequent figures.

studied within the literature is the $c(2\times 2)$ equilibrium order [3–8]. In Fig. 6 we present the entropy evolution for systems with an initial $p(2\times 1)$ order and lateral interaction energies of $\Delta_l=0.1$ (solid), 0.2 (dashed), and 0.4 eV (dotted line), with $\Delta_d=0$ ($N_s=800\times 800$), that correspond to the $c(2\times 2)$ equilibrium order [16]. A further curve with $\Delta_l=0.05$ eV is added (thick solid line, with $N_s=200\times 200$),

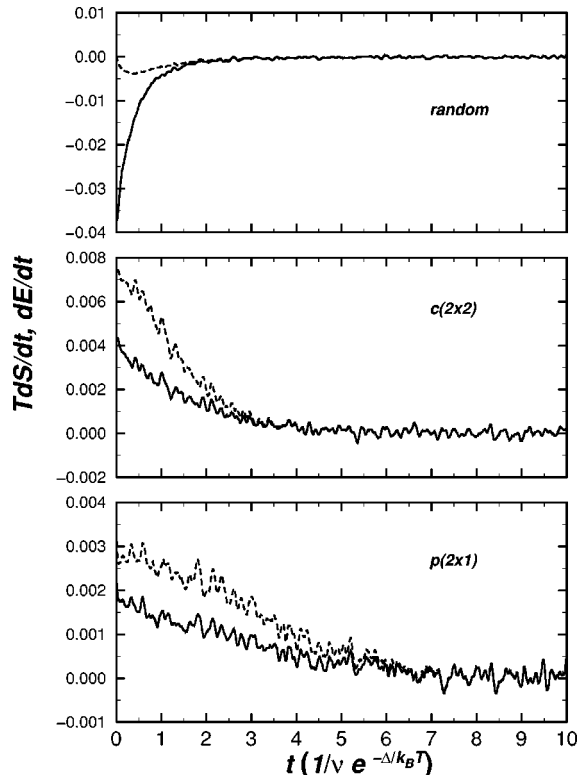


FIG. 5. Time derivatives of the entropy (solid) and internal energy functions (dashed lines) of Fig. 4, for the randomly disordered, $c(2\times 2)$ and $p(2\times 1)$ initial states (top to bottom).

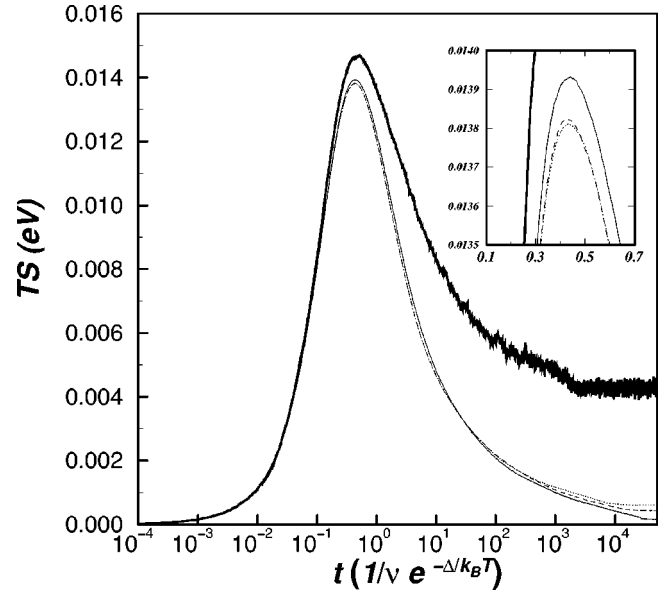


FIG. 6. Time evolution of entropy from an initial $p(2\times 1)$ state for $\Delta_d=0$ and $\Delta_l=0.1$ (solid), 0.2 (dashed) and 0.4 eV (dotted line), with closely matched curves that converge to the $c(2\times 2)$ ordered state. The thick solid curve shows the results for $\Delta_l=0.05$ eV, which converges to a partial $c(2\times 2)$ order.

leading to a slightly different equilibrium state, where the $c(2\times 2)$ order is present but not dominant as in the other curves [34]. The time scale in the time axis is logarithmic, accounting for the fact that the convergence to the $c(2\times 2)$ equilibrium state looks like a long-term power-law decay, and allowing also one to detail the processes in their initial stages. It can be seen that the three $c(2\times 2)$ curves practically collapse into a single one in both the rising phase, from the original zero-entropy state to close to the maxima, and also in the decay phase towards zero entropy, except for their slightly different maxima and some variations for larger times, that are related to the maxima (an inset is included to detail this region). The breaks at $t\approx 5\times 10^3$ are related to the finite size of the lattice. The fourth curve grows with the others in the initial stages, but then arrives at a slightly higher entropy maximum, and finally converges to its own equilibrium state.

The relative insensibility observed in the curves in Fig. 6 to the magnitude of the interaction energies implies that the order destruction and reconstruction mechanisms acting here depend principally on adsorbate jumps with equal transition rates, as a composed process will usually proceed with the slowest rate. From Eq. (3) this means adsorbate jumps to equal and lower energy positions. The initial rise in the entropy corresponds to the destruction of the original $p(2\times 1)$ order, and Fig. 7(a) describes the probable mechanism occurring at the very initial stages. The simplest events given here are a and b , both with an energy difference of $-\Delta_l$ and thus a transition has a rate of $\nu \exp(-\Delta/k_B T)$, and their reverse processes have the rate $\nu \exp[-(\Delta+\Delta_l)/k_B T]$. After the jump in a , the adsorbate may follow the corridor upwards (c) or downwards (c'), with respective energy differences $+\Delta_l$ and $+2\Delta_l$ (once b occurred), which means that it is in a trapped position, and also avoiding jumps to its neighboring empty positions. The single occurrence of a

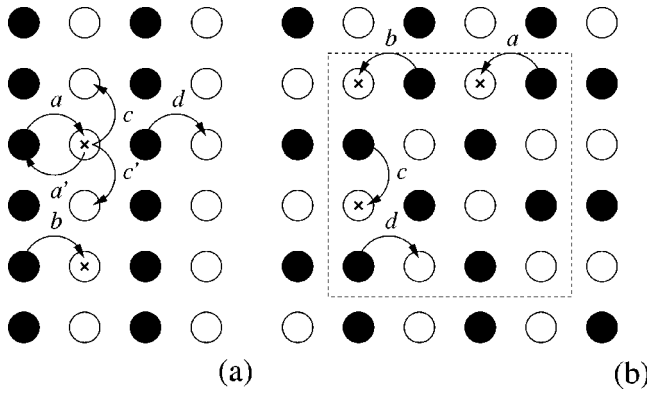


FIG. 7. Probable mechanisms for the common behavior of the curves in Fig. 6, corresponding to the initial rise in entropy due to the destruction of the $p(2 \times 1)$ order (a) and the homogenization of different $c(2 \times 2)$ domains (b). The black and white circles represent, respectively, the occupied and empty sites, and the crosses represent occupied sites after a given event has occurred. Explanation for the mechanisms is given in the text.

does not enhance the possibilities of event d to occur, but it makes much more improbable for its reverse process, and in this way a “checkerboard” order is rapidly formed and stabilized in the local neighborhood [13]. This basic mechanism is also valid for the non- $c(2 \times 2)$ case, but its further divergence means that in this case the $c(2 \times 2)$ domains are not so readily formed and stable as in the combined curves.

The $c(2 \times 2)$ state is twofold degenerate, and this means that the entropy maxima represent the points where there is also a maximum competition between the two different modes, whereas the steady decay of entropy implies that one of them is gradually becoming dominant. A possible mechanism for the decay phase in the $c(2 \times 2)$ curves is shown in Fig. 7(b), where a “block” of the minority mode is surrounded by the dominant one (dashed square). The reordering process should occur with more probability at the borders, where events a and b and d may occur quite rapidly, since they involve no energy differences, but event c may occur with the highest rate only after b or d happened, and any of these will also help to stabilize the lattice further on. The whole process is in fact independent of Δ_l , and the instantaneous decay rate will depend on the total boundary perimeter between the two clusters, and hence the power-law behavior in the decay phase [Fig. 8(a)]. Of course, we may not ignore the diffusion of adsorbates along the defects of the $c(2 \times 2)$, until they are “annihilated” at the borders [5,8], and this process is dependent on the interaction energies, but it is in fact a complementary process, that does not contribute directly to the lattice order as measured by the entropy function. The inclusion of a diagonal term might not be significant, as far as $\Delta_d < 0$, as can be inferred from Fig. 7.

Figure 8(a) presents the results for the entropy (dashed line) and internal energy (solid line) for the case $\Delta_l = 0.2$ eV of Fig. 6, and a logarithmic scale was used in both axes in order to detail the long-time decay (the divergence at the end is a size effect). Both curves run approximately parallel for $t \gtrsim 10$, with a power-law-like behavior $\sim at^{-b}$ [35]. It can be seen from this plot that condition (1) is fulfilled. Figure 8(b) shows the time evolution of the fractions $\tau_2 t_2$ (also $\tau_5 t_5$, dotted line), $\tau_3 t_3$ (solid line), and $\tau_4 t_4$ (dashed line) given in

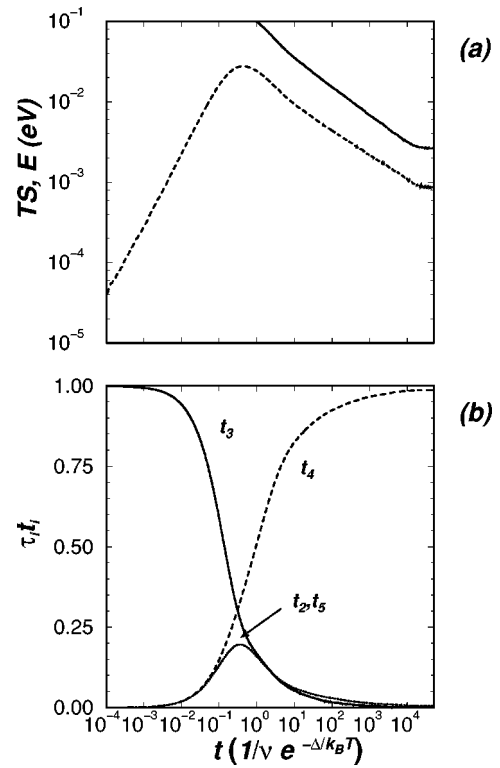


FIG. 8. (a) Power-law-like behavior for the internal energy (solid) and entropy functions (dashed line) for the case $\Delta_l = 0.2$ eV of Fig. 6. (b) Time evolution of the cluster probabilities $\tau_2 t_2$ (or $\tau_5 t_5$, dotted), $\tau_3 t_3$ (solid), and $\tau_4 t_4$ (dashed line) for the same process as (a).

Table I, for the same run. The t_3 and t_4 figures represent, respectively, the $p(2 \times 1)$ and $c(2 \times 2)$ orders, while the t_2 (and t_5) figures represent the immediate disordering state. It can be seen that there is a crossover of the t_3 and t_4 curves at around the entropy maximum, after which t_4 is dominant, and also that the intermediate states t_2 and t_5 have a small maximum at exactly this point, but that the $p(2 \times 1)$ order is still present to some extent up to very large times.

A final case of interest, related to the situations presented above, is the inverse case, i.e., the evolution from an initial $c(2 \times 2)$ state towards the $p(2 \times 1)$ order [9,11]. The time evolution of the entropy is shown in Fig. 9 for $\Delta_d = 0.1$ (solid), 0.2 (dotted), 0.3 (dashed), and 0.4 eV (dot-dashed line), and $\Delta_d = 0$, corresponding to equilibrium $p(2 \times 1)$ orders. A further curve with $\Delta_d = 0.05$ eV is also added (thin solid line), for comparison, but corresponding to a non- $p(2 \times 1)$ order in the equilibrium. The first four curves grow together from the initial zero entropy up to a common maximum at $t \approx 0.2$, and then decay yet together until $t \approx 15$, where they start to diverge due to effect of the different interaction energies, showing that further reordering becomes more difficult the larger the magnitude of the interaction energies is, and they are expected to converge to the ordered state in further times (out of scale). The partial coincidence of the curves means, roughly speaking, that three different ordering phases are present here, and where the first two are energy independent. The non- $p(2 \times 1)$ curve has an identical behavior up to the common maximum, but then falls to its own equilibrium state. Just to note, a main difference between the $c(2 \times 2)$ and $p(2 \times 1)$ orders is that the

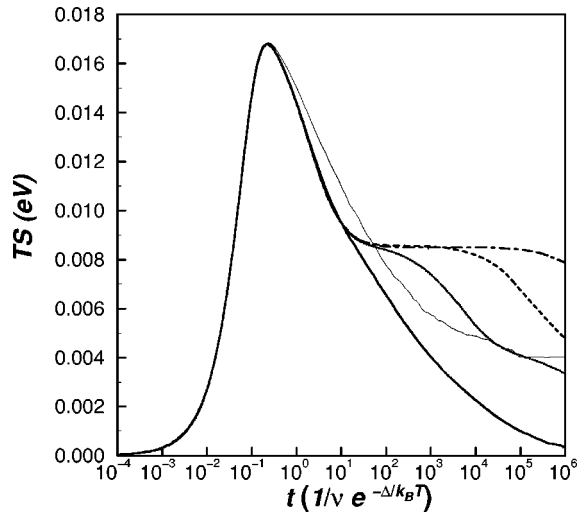


FIG. 9. Time evolution of entropy for an initial $c(2 \times 2)$ order with $\Delta_l = 0$ and $\Delta_d = 0.1$ (solid), 0.2 (dotted), 0.3 (dashed), and 0.4 eV (dot-dashed line), leading to a $p(2 \times 1)$ equilibrium state, and $\Delta_d = 0.05$ eV (thin solid line), leading to partial $p(2 \times 1)$ equilibrium.

first one is twofold, whereas the second one is fourfold degenerate, and therefore a much slower convergence might be expected.

A possible mechanism for the initial disordering phase is shown in Fig. 10(a), where event a can occur as a rapid process (energy difference of $-4\Delta_d$), but its inverse event (a') as a very slow one. Once a has occurred, both b and b' become less probable, with an energy increase of $+\Delta_d$, but favoring c , and thus allowing the formation of local $p(2 \times 1)$ domains, without an explicit energy dependence. The next process should be the homogenization between domains differing by a translational phase, as shown in part (b). Here, events a , b , and c will occur with the same rate, even though event a is not favorable to the order reconstruction, but once event c occurs, for instance, d (that otherwise would be similar to a) is now less probable ($+\Delta_d$), and thus e is favored (zero energy). A combination of the mechanisms of Figs. 10(a) and 10(b) should be responsible for the destruction of the original $c(2 \times 2)$ order and the buildup of small $p(2 \times 1)$ domains, through the maxima of the curves and until they start to diverge at $t \approx 10$ [noting that the non- $p(2 \times 1)$ curve starts to diverge after their common maximum].

The divergence of the curves after their breaking point means that the reordering will now start to depend strongly on the value of the interaction energies, and it is consistently slower with increasing energy. The reordering process should now overcome the mismatch between domains of different orientation, as shown in Fig. 10(c), where we may assume that the domain at the left will expand towards the right. In the simplest mechanism that can be visualized here, event a may occur with a rate $\sim \exp(-2\Delta_d/k_B T)$, and it may be followed by a second jump, b , that will effectively extend the left domain with the maximum rate. Another mechanism is given by events c and d , but with much slower rates (energy differences of $+4\Delta_d$ and $-\Delta_d$).

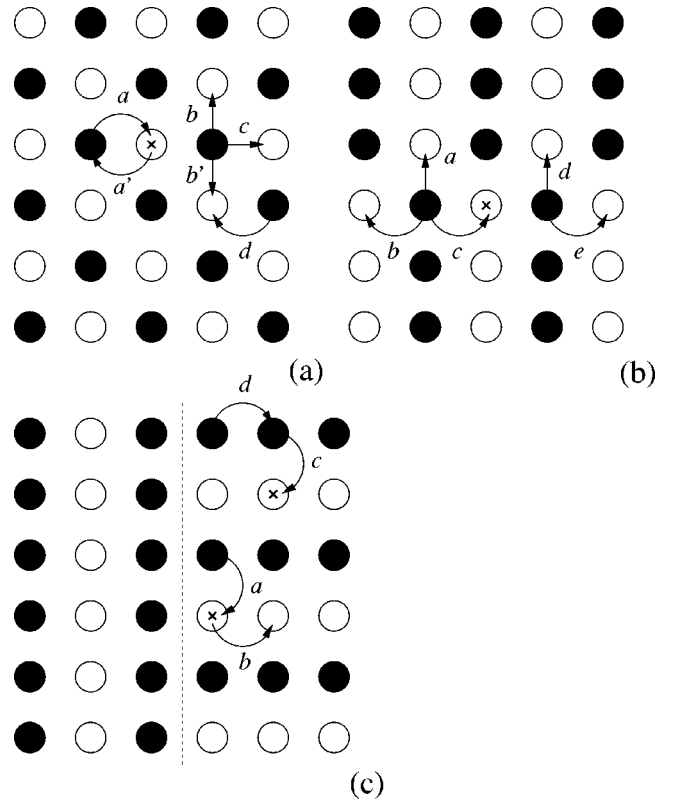


FIG. 10. Possible mechanism for the ordering kinetics in Fig. 9, corresponding to the destruction of the initial $c(2 \times 2)$ order (a), the homogenization of different domains of the $p(2 \times 1)$ order with the same orientation (b), and finally the homogenization of domains with different orientation (c). Mechanism (c) is dependent on the magnitude of the interaction energies. The symbols used here are the same as in Fig. 7.

V. CONCLUSIONS AND FINAL REMARKS

In this work we have analyzed the reordering kinetics of lattice-gas systems with nearest- and next-nearest-neighbor interactions between adsorbates on a square lattice and stochastic hopping (Kawasaki dynamics), from initial predefined ordered states towards the equilibrium, using a dynamic Monte Carlo procedure, so that a “real” time can be evaluated from the local transition rates and the number of possible events in the system at each instant. From the system configuration we can calculate directly the internal energy, and the configurational entropy within the C_2 approximation of the cluster variation method. Within this approach the time variation of both state functions can be directly assessed and thus used to characterize the ordering convergence. The lattice-gas model serves thus as a simple system where the reordering kinetics can be followed and characterized by the state functions in nonequilibrium. From a simple argument on the Helmholtz free energy, we find that the decrease in the internal energy should always be lower than the decrease in entropy, which is confirmed by the simulations. The discussion here was limited to repulsive energies and half coverage, which were used due to richness of phase transitions that this domain can present in equilibrium [20,21].

It was shown that the reordering kinetics varies strongly with the interaction energies, and that the reordering path

may depend more on the initial and final orders of the process than on the magnitude of the interaction energies themselves. From the entropy function and the order parameters we can also identify different ordering phases corresponding to the destruction of the initial order and the buildup of the equilibrium state. Two extreme cases presented here are those where the system evolves from a $p(2 \times 1)$ state towards a $c(2 \times 2)$ state (Fig. 6), and the opposite process (Fig. 9), where we can perceive an “insensibility” of the entropy function to the magnitude of the interactions as long as the equilibrium state is unchanged, and the different ordering-disordering phases are well characterized in the entropy variation. At this point a comparison with Smith and Zangwill [13] is relevant: they observe in their calculations for ordering processes that the short-range order converges very rapidly to a *quasiequilibrium* state, after which the long-range order converges exponentially and both orders relax to their equilibrium state. This can be interpreted in our system as the initial formation of the local domains and their subsequent “annealing” into the final order. The model of Ref. [13] is, despite its elegance, limited by the use of a quasi-chemical approximation, that can only account for local correlations and cannot describe properly the $c(2 \times 2)$ and $p(2 \times 1)$ ordered states [16], and thus the advantage of the Monte Carlo method. On the other hand, entropy was chosen as a single function that will characterize the order of the system as a whole.

The reordering kinetics cannot be directly related to the diffusion kinetics in the equilibrium, but this does not mean that diffusion is absent or unimportant for reordering. In fact,

as discussed for the $c(2 \times 2)$ case, the diffusion within the ordered domains is important as a complementary process for “defect” transportation that does not necessarily change the order measure, while the reordering process itself will occur at the borders of the domains. The cases studied here included well defined ordering states, like the $c(2 \times 2)$ and $p(2 \times 1)$, that are perhaps rather “artificial,” but they allow the discussion of some possible mechanisms for the kinetics of order formation and destruction, and how these will be expressed by the state functions.

Even though the analysis presented here is limited due to the finiteness of the systems studied, its related fluctuations, and also on other factors like the definition of the hopping rules and the simplicity of cases studied, the Monte Carlo procedure outlined above can be fairly extended to more realistic cases for the reordering kinetics of an adsorbate layer, and also its relation to other nonequilibrium processes where competing time scales are involved, like adsorption, desorption and surface reactions, or external effects like varying temperatures or applied external fields.

ACKNOWLEDGMENTS

The author acknowledges financial support from the Fundação de Amparo à Pesquisa do Estado de São Paulo (FAPESP) (Brazil), Project No. 96/06416-7, and the computational facilities accessible to him at the Institute for Computer Applications 1 of the University of Stuttgart. The author is also very grateful for the early encouragements and critical comments by Claudio Scherer and Stefan Luding.

-
- [1] H. C. Kang and W. H. Weinberg, *J. Chem. Phys.* **90**, 2824 (1989).
 - [2] A. M. Bowler and E. S. Hood, *J. Chem. Phys.* **94**, 5162 (1991).
 - [3] P.-L. Cao, *Phys. Rev. Lett.* **73**, 2595 (1994).
 - [4] P.-L. Cao, M. Qiu, and L.-Q. Lee, *J. Phys.: Condens. Matter* **8**, 1335 (1996).
 - [5] G. E. Murch, *Philos. Mag. A* **43**, 871 (1981).
 - [6] C. Uebing and R. Gomer, *J. Chem. Phys.* **95**, 7626 (1991).
 - [7] C. Uebing and R. Gomer, *Ber. Bunsenges. Phys. Chem.* **100**, 1138 (1996).
 - [8] C. Uebing, V. Pereyra, and G. Zgrablich, *J. Chem. Phys.* **106**, 9320 (1997).
 - [9] C. Uebing and R. Gomer, *Surf. Sci.* **381**, 33 (1997).
 - [10] Y. He and R. B. Pandey, *Phys. Rev. Lett.* **71**, 565 (1993).
 - [11] A. Szolnoki, G. Szabó, and O. G. Mouritzen, *Phys. Rev. E* **55**, 2255 (1997).
 - [12] R. Gomer, *Rep. Prog. Phys.* **53**, 917 (1990).
 - [13] J. R. Smith Jr. and A. Zangwill, *Surf. Sci.* **316**, 359 (1994).
 - [14] B. Meng and W. H. Weinberg, *J. Chem. Phys.* **100**, 5280 (1994).
 - [15] B. Meng and W. H. Weinberg, *J. Chem. Phys.* **102**, 1003 (1995).
 - [16] S. Weinketz and G. G. Cabrera, *J. Chem. Phys.* **106**, 1620 (1997).
 - [17] R. Kikuchi, *Phys. Rev.* **81**, 988 (1951).
 - [18] R. Kikuchi and S. G. Brush, *J. Chem. Phys.* **47**, 195 (1967).
 - [19] S. H. Payne, H. J. Kreuzer, and L. D. Roelofs, *Surf. Sci. Lett.* **259**, L781 (1991).
 - [20] K. Binder and D. P. Landau, *Phys. Rev. B* **21**, 1941 (1980).
 - [21] K. Binder and D. P. Landau, *Surf. Sci.* **108**, 503 (1981).
 - [22] K. Binder and D. Stauffer, in *Applications of the Monte Carlo Method in Statistical Physics*, Vol. 4 of *Topics in Current Physics*, 2nd ed., edited by K. Binder (Springer-Verlag, Berlin, 1987).
 - [23] P. W. Atkins, *Physical Chemistry*, 5th ed. (Oxford University Press, Oxford, 1994).
 - [24] N. Metropolis *et al.*, *J. Chem. Phys.* **21**, 1087 (1953).
 - [25] K. A. Fichthorn and W. H. Weinberg, *J. Chem. Phys.* **95**, 1090 (1991).
 - [26] D. T. Gillespie, *J. Phys. Chem.* **81**, 2340 (1977).
 - [27] K. J. Laidler, *Chemical Kinetics*, 3rd ed. (Harper and Row, New York, 1987).
 - [28] B. E. Cooper, *Statistics for Experimentalists* (Pergamon Press, Oxford, 1969).
 - [29] W. H. Press, S. A. Teukolsky, W. T. Vetterling, and B. P. Flannery, *Numerical Recipes in FORTRAN: The Art of Scientific Computing*, 2nd ed. (Cambridge University Press, Cambridge, 1992).
 - [30] A. B. Bortz, M. H. Kalos, and J. L. Lebowitz, *J. Comput. Phys.* **17**, 10 (1975).
 - [31] Note that $\int_0^1 (-\ln \rho) d\rho = 1$, and therefore $-\ln \rho$ represents the uncertainty about the time interval between two events in the Poisson process.

- [32] D. de Fontaine, *Configurational Thermodynamics of Solid Solutions, Solid State Physics* (Academic Press, New York, 1979).
- [33] A. H. W. Beck, *Statistical Mechanics, Fluctuations and Noise* (Edward Arnold, London, 1976).
- [34] The $c(2 \times 2)$ order at half coverage, in the absence of next-nearest-neighbor interactions, should appear for $\Delta_I/k_B T \geq 1.76$ [19,21,16], which corresponds here to $\Delta_d \geq 0.045$ eV. The value for the last curve, $\Delta_I = 0.05$ eV, falls slightly above this point, but the different equilibrium state can be justified by recognizing a second-order transition in the onset of the $c(2 \times 2)$ order, as found within the C_2 approximation of the CVM [16].
- [35] In the region $10 \leq t \leq 10^3$ we find for TS , $a = 0.009\,561\,01$ and $b = 0.318\,533$, and for E , $a = 0.039\,693\,5$ and $b = 0.357\,411$, indicating that their decay rates are very similar.